Symmetry Collapse due to the Presence of Worm-Aromaticity in Ge_{24}^{4-}

Hong-Lei Xu
Nankai University
Nikolay Tkachenko
Utah State University https://orcid.org/0000-0002-7296-4293
Alvaro Muñoz-Castro
Universidad Autónoma de Chile
Alexander Boldyrev (a.i.boldyrev@usu.edu)
Utah State University https://orcid.org/0000-0002-8277-3669
Zhong-Ming Sun
Nankai University https://orcid.org/0000-0003-2894-6327

Article

Keywords: X-ray Diffraction Analysis, Energy-dispersive X-ray Spectroscopy, Electron Delocalization, Prolate Cluster, Independent Shielding Cones, Global Symmetry

Posted Date: May 21st, 2021

DOI: https://doi.org/10.21203/rs.3.rs-482672/v1

Abstract

In this work, we synthesized and isolated a continuous 24-atom cluster Ge_{24}^{4-}, which was characterized by X-ray diffraction analysis and Energy-dispersive X-ray spectroscopy, showing an elongated worm-like structural characteristic. Theoretical analysis reveals that electron delocalization plays a vital role in the formation and stabilization of the prolate cluster. In contrast with carbon atoms, 4s orbitals of Ge-atoms do not easily hybridize with 4p orbitals and s-type lone-pairs could be localized with high occupancy. Thus, there are not enough electrons to form a stable symmetrical fullerene-like structure such as C_{24} fullerene. Three aromatic units with two [Ge_9] and one [Ge_6] species, connected by classical 2c-2e Ge-Ge σ-bonds, have been aligned together forming three independent shielding cones (worm-aromaticity) and eventually caused a collapse of the global symmetry of the prolate cluster.

Summary Paragraph

Large continuous cluster of germanium Ge_{24}^{4-} was isolated in a solid state and experimentally characterized by X-ray diffraction analysis and Energy-dispersive X-ray spectroscopy. The Ge_{24}^{4-} cluster not only confirms the structural evolution trends theoretically predicted before in a gas phase, but also sheds light on the grounds of the low symmetry of the structure. The Adaptive Natural Density Chemical Partitioning (AdNDP) and magnetic response analyses clearly indicate the presence of three aromatic fragments aligned together, featuring a new type of aromaticity in chemistry - worm-aromaticity.

Main Text

Understanding how the addition of atoms one by one leads to the transition from a single atom to a diatomic molecule to atomic clusters and finally to the formations of bulk solid-state allotropes is a dream of many chemists. This understanding will help us to design new tailorable materials with ever unusual structures and other physical and chemical properties. Today we still do not understand how such evolution is happening. A striking example is a carbon - one of the most investigated elements. Although it is known that the transition from diatomic C_2 to larger carbon clusters goes through the formation of linear chains,[1] cyclic structures,[2] and cage-like fullerenes,[3] we still do not completely know how fullerenes will transform upon further addition of atoms and finally form bulk graphite or diamond. For other elements, our knowledge of this evolution is less clear. Even for the most similar isoelectronic elements of the IV group of the Periodic Table (Ge and Si), computational studies showed that atomic clusters' structures behave differently upon growth.[4-6] Thus, the smallest fullerene-like structure for carbon atom occurs at 20 atoms[7] and continues to evolve beyond. However, according to the computational results, Si and Ge tend to form prolate structures for medium-sized clusters rather than spherical-like fullerenes. The experimental evidence of such behavior so far was limited to ion mobility experiments[8] and 2D electron microscopy experiments.[9] Although theory can propose some trustworthy candidates for low energy structures, one of the most reliable piece of experimental evidence - a solid state X-Ray characterization, is still lacking for large continuous Ge clusters. Hence the isolation of

medium-sized germanium species as a key intermediate to understand the structural transition is of greatest importance. The isolated germanium clusters with over 10 atoms known to date are always exhibited a sole coupling model of small clusters,[10-12] which should be better regarded as polymerization tendency but not a structural evolution. Herein, we report the successful isolation and structural characterization of a germanium cluster Ge_{24}^{4-} (**1a**) featuring an extended worm-like structure with fused three-fold faces. Our theoretical calculations showed that Ge_{24}^{4-} consists of three independent sigma- or spherically aromatic fragments, which is the reason for the collapse of the symmetry and the formation of a prolate structure. This result helps us to understand why carbon structures are so different from silicon, germanium ones. Such a model of Ge_{24}^{4-} reveals the real structural features of medium-sized germanium clusters providing solid prospects for further rationalization of larger species.

The title complex $[K(2,2,2\text{-crypt})]_4Ge_{24}$ (**1**) was synthesized by mild oxidation of $K_{12}Ge_{17}$ using excess $Co(dppe)Cl_2$ in ethylenediamine solutions at 55 °C. After layered with toluene for 5 weeks, black block-like crystals occurred on the wall of a reaction test tube in an approximate 25% yield based on $K_{12}Ge_{17}$. The as-synthesized **1** could not be reproduced by using other cobalt reagents such as $CoMes_2$ or tuning down the reaction temperature, otherwise, only some small Ge clusters such as $[K(2,2,2\text{-crypt})]_2Ge_9$ and $[K(2,2,2\text{-crypt})]_2Ge_5$ were afforded. Energy-dispersive X-ray spectroscopy (EDX, Figure S8) displayed the composition of **1**, including only two (semi)metal elements of K and Ge, which is in good agreement with the calculated values. Electrospray-ionization mass spectrometry by dissolving crystals of **1** in DMF solution indicated a corresponding weak signal of parent cluster was observed at *m/z*= 2989.7936 for $\{[K(2,2,2\text{-crypt})]_3[Ge_{24}]\}^-$.

As shown in Fig. 1A, the overall structure of Ge_{24}^{4-} is prolate with an aspect ratio of nearly 3:1 and can be divided into four different polyhedron sections, including a D_{3h}-symmetric Ge_9 cage (**unit-1,** Ge1-9), distorted prism (**unit-2,** Ge7-12), second peculiar Ge_9 cage (**unit-3,** Ge10-18) and the third distorted C_{4v}-symmetric Ge_9 cage (**unit-4,** Ge16-24). In light of the structural feature, cluster **1a** may undergo a complex growth from the small species. From another perspective, it could also be described as two-terminal Ge_9-units bridged via a Ge_6 central fragment along *exo*-bonds to triangular faces. In this sense, the central bowl-shaped Ge_6 fragment plays a crucial role in the formation of **1a**, and it is suggested as a growth-trigger in the evolution towards larger species. Furthermore, it is also likely to affect the shapes of two terminal Ge_9-cages by the different coordination fashions. The whole structure can be also viewed as three connected Ge_9-units involving a terminal cage and fused nine-membered cages sharing three atoms, providing many flavors of the Ge Zintl-ion chemistry in a single molecular structure, able to coincide under similar experimental conditions.

The bowl-shaped Ge_6 fragment (Fig. 1B) is reminiscent of similar organic molecules corannulene ($C_{20}H_{10}$)[13] or sumanene ($C_{21}H_{12}$)[14], a fullerene fragment, with a curved molecular surface. In contrast, the bowl depth of the Ge_6 fragment is 0.93 Å, which is close to corannulene (~0.88 Å).[15] As shown in Fig. 1C,

the central triangle (dotted lines) in the Ge_6 fragment has elongated Ge-Ge distances of av. 2.813 Å like $[Au_3Ge_{45}]^{9-}$,[16] which is remarkably longer than other Ge-Ge bonds with an average length of 2.487 Å. Furthermore, the Ge_6 bowl combines with a neighboring Ge_3 face from **unit-4** by three Ge-Ge bonds (2.471-2.495 Å) to form an interesting nine-atom cage (Fig. 1D) in which two staggered Ge_3 faces lead to three almost identical edge-sharing pentagons. In **unit-1**, the Ge-Ge distances (2.5304(16)-2.6739(16) Å) are in the normal range[17] and lengths of the prisms (Ge1–Ge7, 2–8, 3–9: 2.8084(16)–2.8744(16) Å) are elongated compared with those (2.71–2.73 Å) in bare D_{3h}-$[Ge_9]^{2-}$ cluster.[18] Additionally, the extended bottom face of the central Ge_6 fragment coordinates to the triangle face of **unit-1** through three *exo* Ge-Ge bonds (av. 2.581 Å) forming a distorted triangular prism (Fig. 1E). In contrast to D_{3h}-**unit-1**, **unit-4** exhibits a largely distorted C_{4v}-structure with a broader range of Ge-Ge contacts (2.4960(14)-2.8598(15) Å).

To understand the reason for the stability and geometrical features of the Ge_{24}^{4-} we performed density functional theory (DFT) calculations.[19-20] The details of theoretical calculations are given in the Supporting Information file. The optimized geometry resembles all structural features that were found in the X-Ray experiment. The average Ge-Ge distance of the optimized structure is 0.07 Å longer than the experimental one, which is a common deviation for the calculation of highly charged Zintl ions with DFT methods. A high HOMO-LUMO gap (2.61 eV) was found for the optimized cluster indicating its remarkably high stability. To analyze chemical bonding of the synthesized cluster, we performed the Adaptive Natural Density Partitioning (AdNDP) analysis.[21-22] The AdNDP is an electron-localization technique that partition the natural density of the system and reproduces the most occupied localized bonding elements. The results of the analysis are shown in Fig. 2. We start our localization from one-center two-electron (1c-2e) elements and found fifteen s-type lone-pairs with high occupancy number (ON = 1.90-1.87 |e|) on Ge-atoms. Chemical bonding of the middle part of the cluster majorly consists of classical 2c-2e Ge-Ge σ-bonds with ON = 1.95-1.91 |e| and provides a binding between Ge_6 and two Ge_9 fragments. Highly occupied delocalized 3c-2e σ-bond (ON = 1.96 |e|) governs the binding within Ge_6 fragment and stabilizes the bowl-like Ge_6 structure. Chemical bonding of D_{3h}-Ge_9 fragment consists of two 3c-2e σ-bonds with ON = 1.97 |e| and nine 5c-2e σ-bonds (three bonds per each Ge_5 cap) with ON = 1.91-1.79 |e|. The collection of such delocalized bonding elements possesses spherical-like shielding cones as was shown in our previous studies.[23-24] Analogically, the chemical bonding of the C_{4v}-Ge_9 fragment consists of three delocalized bonding regions resulting in three 5c-2e bonding elements within the Ge_5 cap (ON = 1.98-1.93 |e|), three 4c-2e bonding elements within the Ge_4 square (ON=1.95-1.62 |e|), and five 8c-2e bonding elements within the Ge_8 antiprism (1.99-1.87 |e|). Shapes of found bonds and numbers of electrons on the fragments that agree with the Hückel's (4n+2) electron counting rule render two Ge_9 fragments as locally σ-aromatic fragments.[25] From the chemical bonding analysis described above, we can expect the presence of three independent aromatic regions from C_{4v}-Ge_9, Ge_6, and D_{3h}-Ge_9 fragments.

In order to explore the aromatic characteristics of **1a**, the magnetic criteria of aromaticity were evaluated via the induced magnetic field ($\mathbf{B}^{ind}$) (Fig. 3a).[26-28] The averaged (isotropic) term, given by $\mathbf{B}_{iso}^{ind}$=-(1/3)(s_{xx}+s_{yy}+s_{zz})$\mathbf{B}_j^{ext}$, shows a continuous shielding region along with the entire structure. Significantly, under different orientations of the applied field, the shielding cone characteristics were found. In contrast to planar aromatic species for which shielding cones are enabled only when the field is oriented perpendicular to the ring,[29] we found the presence of three cones merged together for any direction of the applied field.[28,30] With the field-oriented along the axis containing all the three cluster fragments (*i.e. z*-axis), a formation of three-overlapped shielding cones centered at each Ge-fragment is observed. For perpendicular orientations (*i.e. y*- and *x*-axis), the three shielding cones are aligned similar to the anthracene molecule featuring three fused aromatic rings.[31] Such features are retained under arbitrary orientations of the applied field, denoting how the three adjacent shielding cones evolve under rotation (Fig. S9).

Next, we explore the characteristics of each aromatic unit. To represent Ge_6 bowl-like structure, a Ge_9 cluster with a shared triangular face of C_{4v}-Ge_9 was chosen. Interestingly, despite of fragments' different shapes, each isolated fragment exhibits similar characteristics to spherical aromatic species with a continuous shielding region from $\mathbf{B}_{iso}^{ind}$, and shielding cone characteristics under different orientations of the field (Fig. 3B).[29] Noteworthy, the overlap between the aromatic characteristics of the three isolated Ge_9^{4-} clusters largely resembles the behavior of the overall Ge_{24}^{4-} cluster supporting that after aggregation involving both *exo*-bonds and face-fusion schemes, each Ge_9 unit meets the electronic distribution requirements to behave as spherical aromatics. Hence, Ge_{24}^{4-} is the first example of a linear trimer built-up by related spherical or sigma-aromatic clusters, exhibiting different shapes and aggregation schemes. We called such an alignment of spherically-aromatic shielding cones – worm-aromaticity.

The synthesis and characterization of a worm-like Ge_{24}^{4-} cluster in a solid-state is a missing chain link between small germanium clusters and bulk solid-state germanium. It confirms the structural evolution trends that were predicted computationally in a gas phase, providing an explicit structural characteristic of a previously unknown medium-sized Ge cluster. High symmetry collapse in Ge_{24}^{4-} occurs due to the presence of worm-aromaticity and lack of s-p hybridization in Ge. The formation of three independent spherically aromatic units shed light on the reason for the formation of low-symmetric prolate structure. We expect that this new kind of aromaticity will be found in many cluster chemical compounds made in the future. We believe that the further investigation of the transition from atomic clusters to bulk materials will bring an understanding and a significant advancement for materials design with a target physical property.

Methods

All manipulations and reactions were performed under a dry nitrogen atmosphere in glove box. Ethylenediamine (Aldrich, 99%) and DMF (Aldrich, 99.8%) used in experiments were freshly distilled by CaH_2 prior to use. Toluene (Aldrich, 99.8%) was distilled from sodium/benzophenone under nitrogen and stored under nitrogen. 2,2,2-crypt (4,7,13,16,21,24-Hexaoxa-1,10-diazabicyclo (8.8.8) hexacosane, purchased from Sigma-Aldirich, 98%) and Co(dppe)Cl_2 (purchased from Alfa Aesar, ≥97%) were dried in vacuum for 12 h prior to use. The Zintl phase $K_{12}Ge_{17}$ was prepared by heating stoichiometric mixtures of the elements (K and Ge) in sealed niobium containers closed in evacuated quartz ampules according to the reported literature.[32]

1.1 Synthesis of $[K(2,2,2\text{-crypt})]_4Ge_{24}$ (1)

$K_{12}Ge_{17}$ (170 mg, 0.100 mmol) and 2,2,2-crypt (160 mg, 0.424 mmol) were dissloved in 3 mL en in a reaction vial and stirred for 10 min. Co(dppe)Cl_2 (63.4 mg, 0.120 mmol) was added and stirred for 6 h at 55 ℃. The resulting brown-red solution was filtered with standard glass frit and layered with 4 mL toluene. About 35 days later, black block-like crystals **1** was observed in the test tube (25% yield based on $K_{12}Ge_{17}$).

1.3 X-ray Diffraction

Suitable crystal from **1** was selected for X-ray diffraction analysis. Crystallographic data was collected on Rigaku XtalAB Pro MM007 DW diffractometer with graphite monochromated Mo Kα radiation (λ = 0.71073 Å). The structure of crystal **1** was solved using direct methods and then refined using SHELXL-2014 and Olex2.[33-35] All the non-hydrogen atoms were refined anisotropically. All hydrogen atoms of organic groups were rationally placed by geometrical considerations. We used the PLATON SQUEEZE procedure to remove the solvent molecules which could not be modeled properly.[36] We refined the structure by using the rational restrains of anisotropy (SIMU, ISOR, DFIX for K-crypt fragments) and omitted the most disagreeable reflections.

1.4 Electrospray Ionization Mass Spectrometry (ESI-MS)

Negative ion mode ESI-MS of the DMF solution of crystals of **1** was measured on an LTQ linear ion trap spectrometer by Agilent Technologies ESI-TOF-MS (6230). The spray voltage was 5.48 kV and the capillary temperature was kept at 300 °C. The capillary voltage was 30 V. The samples were prepared inside a glovebox and very rapidly transferred to the spectrometer in an airtight syringe by direct infusion with a Harvard syringe pump at 0.2 mL/ min.

1.5 Energy Dispersive X-ray (EDX)

EDX analysis on the title cluster **1** was performed using a scanning electron microscope (FE-SEM, JEOL JSM-7800F, Japan). Data acquisition was performed with an acceleration voltage of 20 kV and an accumulation time of 60 s.

1.6 Quantum Chemical Calculations

Magnetic response analysis: Geometry optimizations and subsequent calculations were performed using scalar relativistic DFT methods employing the ADF code with the all-electron triple-z Slater basis set plus the double-polarization (STO-TZ2P) basis set in conjunction with the PBE0 functional *(19, 37-38)*. In order to evaluate the induced field ($\mathbf{B}^{ind}$) upon an external magnetic field ($\mathbf{B}^{ext}$) at the molecular surroundings, according to $B_i^{ind} = -\sigma_{ij}B_j^{ext}$,[26,39-42] the nucleus-independent shielding tensors (σ_{ij})[26,42-43] were calculated within the GIAO formalism, employing the OPBE[38,44-45] functional and the all-electron triple-z Slater basis set plus the double-polarization (STO-TZ2P), placed in a three-dimensional grid. Relativistic effects were considered through the ZORA Hamiltonian,[46] ensuring an equal footing treatment of different clusters. For convenience, the *i* and *j* suffixes are related to the x-, y- and z-axes of the molecule-fixed Cartesian system (*i,j* = x,y,z). The values of B^{ind} are given in ppm in relation to B^{ext}.

Chemical bonding analysis: Geometry optimization and frequency calculations were performed using Gaussian 16 software at the PBE0/Def2-QZVP level of theory.[20,38,47] To identify the chemical bonding of investigated species, we carried out adaptive natural density partitioning (AdNDP) analysis as implemented in the AdNDP 2.0 code.[21,22] Chemical bonding was analyzed at PBE0/Def2-TZVP level of theory. Previously, AdNDP results have been shown to be insensitive to the size of basis set used.[48]

Declarations

Data availability

The data that support the findings of this study are available from the corresponding authors on a reasonable request.

Acknowledgments

This work was supported by the National Natural Science Foundation of China 21971118 to Z.-M.S.. A.I.B. acknowledges financial support from the R. Gaurth Hansen Professorship fund. The support and resources from the Centre for High Performance Computing at the University of Utah are gratefully acknowledged. A.M.-C. acknowledges financial support from FONDECYT 1180683.

Authors contributions

Z.-M.S. conceived the project and designed the experiments. H.-L.X. performed the synthesis. N.V.T., A.M.-C., and A.I.B. performed the quantum chemical calculations and analyzed the data. All authors co-wrote the manuscript.

Competing interests

The authors declare no competing of interest.

References

[1] A. V. Orden, R. J. Saykally, *Chem. Rev.* **98**, 2313–2358 (1998).

[2] K. Kaiser, *et al., Science* **365**, 1299-1301 (2019).

[3] H. W. Kroto, *et al., Nature* **318**, 162–163 (1985).

[4] S. Yoo, X. C. Zeng, *J. Chem. Phys.* **124**, 184309 (2006).

[5] W.-C. Lu, *et al., Phys. Chem. Chem. Phys.* **12**, 8551-8556 (2010).

[6] L-.Z. Zhao, *et al., Chem. Phys. Lett.* **455**, 225–231 (2008).

[7] H. Prinzbach, *et al., Nature* **407,** 60–63 (2000).

[8] J. M. Hunter, *et al., Phys. Rev. Lett.* **73**, 2063–2066 (1994).

[9] S. Bals, *et al., Nat. Commun.* **3**, 897 (2012).

[10] A. Ugrinov, S. C. Sevov, *Inorg. Chem.* **42**, 5789–5791 (2003).

[11] A. Ugrinov, S. C. Sevov, *J. Am. Chem. Soc.* **124**, 10990–10991 (2002).

[12] C. Downie, Z.-J. Tang, A. M. Guloy, *Angew. Chem. Int. Ed.* **39**, 337-340 (2000).

[13] W. E. Barth, R. G. Lawton, *J. Am. Chem. Soc.* **88**, 380-381 (1966).

[14] H. Sakurai, T. Daiko, T. Hirao, *Science* **301**, 1878 (2003).

[15] A. V. Zabula, *et al., Science* **333**, 1008-1011 (2011).

[16] A. Spiekermann, *et al., Angew. Chem. Int. Ed.* **46**, 5310–5313 (2007).

[17] R. J. Wilson, *et al., Chem. Rev.* **119**, 8506–8554 (2019).

[18] J. Åkerstedt, *et al., Eur. J. Inorg. Chem.* **2011**, 3999–4005 (2011).

[19] C. Adamo, V. Barone, *J. Chem. Phys.* **110**, 6158 – 6169 (1999).

[20] F. Weigend, R. Ahlrichs, *Phys. Chem. Chem. Phys.* **7**, 3297 –3305 (2005).

[21] D. Y. Zubarev, A. I. Boldyrev, *Phys. Chem. Chem. Phys.* **10**, 5207 – 5217 (2008)

[22] N. V. Tkachenko, A. I. Boldyrev, *Phys. Chem. Chem. Phys.* **21**, 9590 – 9596 (2019).

[23] H.-L. Xu, *et al., Nat. Commun.* **11**, 5286 (2020).

[24] H.-L. Xu, *et al., Angew. Chem. Int. Ed. DOI: 10.1002/anie.202102578* (2021).

[25] N. V. Tkachenko, A. I. Boldyrev, *Chem. Sci.* **10**, 5761–5765 (2019).

[26] R. Islas, T. Heine, G. Merino, *Acc. Chem. Res.* **45**, 215–228 (2012).

[27] R. Benassi, P. Lazzeretti, F. Taddei, *J. Phys. Chem.* **79**, 848–851 (1975).

[28] P. R. von Schleyer, H. Jiao, *Pure Appl. Chem.* **68**, 209–218 (1996).

[29] A. Muñoz-Castro, *Phys. Chem. Chem. Phys.* **19**, 12633–12636 (2017).

[30] J. A. Pople, K. G. Untch, *J. Am. Chem. Soc.* **88**, 4811–4815 (1966).

[31] N. D. Charistos, A. Muñoz-Castro, M. P. Sigalas, *Phys. Chem. Chem. Phys.* **21**, 6150–6159 (2019).

[32] H. G. V. Schnering *et al.*, *Z. Anorg. Allg. Chem.* **623**, 1037-1039 (1997).

[33] G. M. Sheldrick, *Acta. Cryst. A.* **71**, 3-8 (2015).

[34] O. V. Dolomanov, L. J. Bourhis, R. J. Gildea, J. A. K. Howard, H. Puschmann, *J. Appl. Crystallogr.* **42**, 339-341 (2009).

[35] A. L. Spek, *Acta. Cryst. D.* **65**, 148-155 (2009).

[36] A. L. Spek, *Acta Crystallogr. Sect. C Cryst. Struct. Commun.* **71**, 9-18 (2015).

[37] Amsterdam Density Functional (ADF 2019) Code, Vrije Universiteit: Amsterdam, The Netherlands. Available at: http://www.scm.com

[38] J. P. Perdew, K. Burke, M. Ernzerhof, *Phys. Rev. Lett.* **77**, 1396–1396 (1996).

[39] M. Baranac-Stojanović, *RSC Adv.* **4**, 308–321 (2014).

[40] S. Klod, E. Kleinpeter, *J. Chem. Soc. Perkin Trans.* **2**, 1893–1898 (2001).

[41] N. D. Charistos, A. G. Papadopoulos, M. P. Sigalas, *J. Phys. Chem. A* **118**, 1113–1122 (2014).

[42] T. Heine, C. Corminboeuf, G. Seifert, *Chem. Rev.* **105**, 3889–3910 (2005).

[43] G. Merino, T. Heine, G. Seifert, *Chem. Eur. J.* **10**, 4367–4371 (2004).

[44] J. P. Perdew, K. Burke, Y. Wang, *Phys. Rev. B* **54**, 16533–16539 (1996).

[45] N. C. Handy, A. J. Cohen, *Mol. Phys.* **99**, 403–412 (2001).

[46] E. van Lenthe, E. J. Baerends, J. G. Snijders, *J. Chem. Phys.* **101**, 9783–9792 (1994).

[47] M. J. Frisch, et al. Gaussian 16, Revision B.01, Gaussian, Inc., Wallingford (2016).

[48] A. P. Sergeeva, A. I. Boldyrev, *Comm. Inorg. Chem.* **31**, 2-12 (2010).

Figures

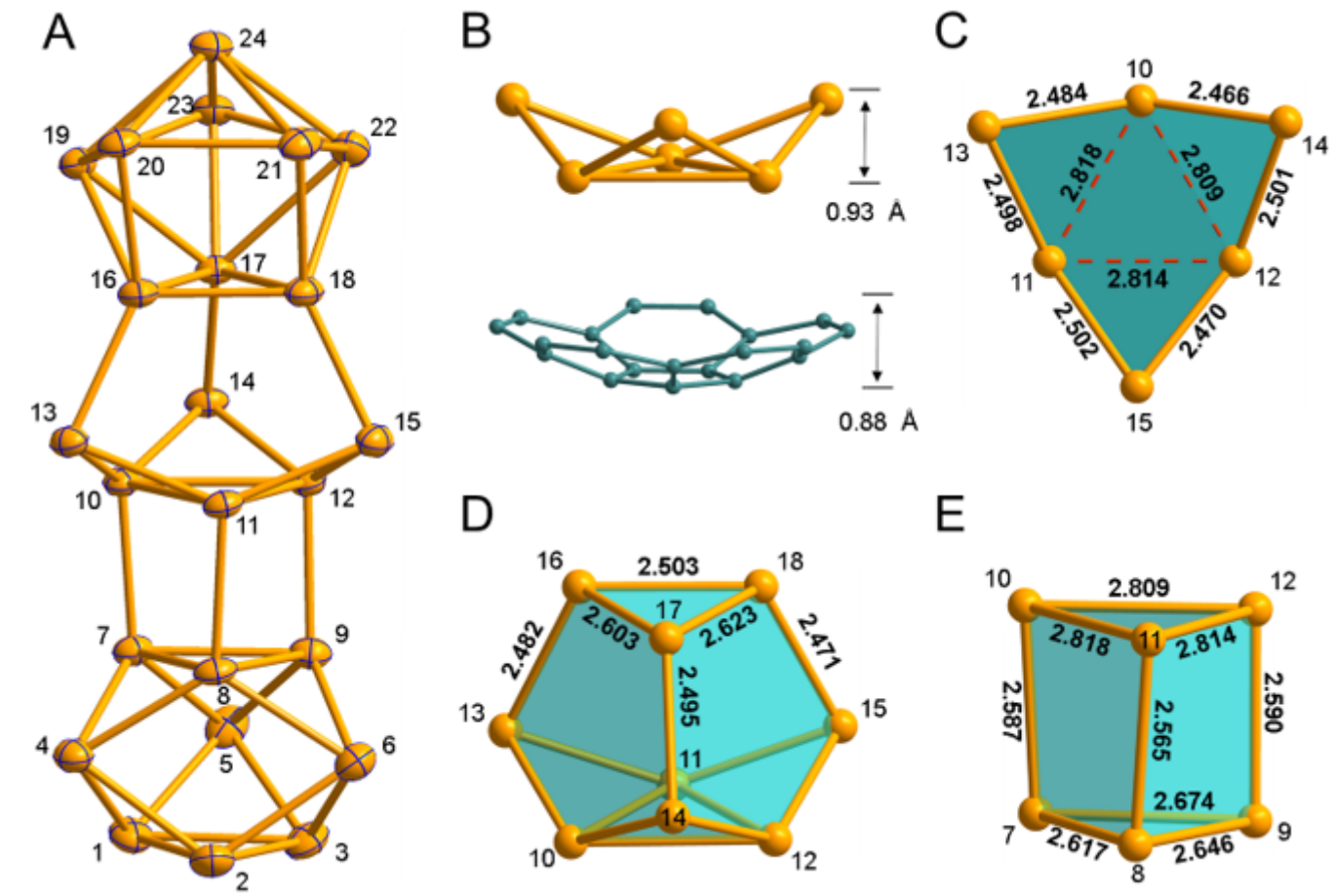

Figure 1

(A) ORTEP representation of cluster Ge244- (1a) at 50% probability. (B) The contrast of bowl-shaped Ge6 fragment (top, Ge10-Ge15) with bowl depth of 0.93 Å and corannulene C20H10 (bottom) with ~0.88 Å. (C) The bowl-shaped Ge6 fragment shown from a vertical view. (D) View of Ge9 cage (Ge10-Ge18). (E) The distorted prism Ge6 fragment consisting of a triangle of Ge7-9 and an extended triangle of Ge10-12. All selected bond lengths are given in Å.

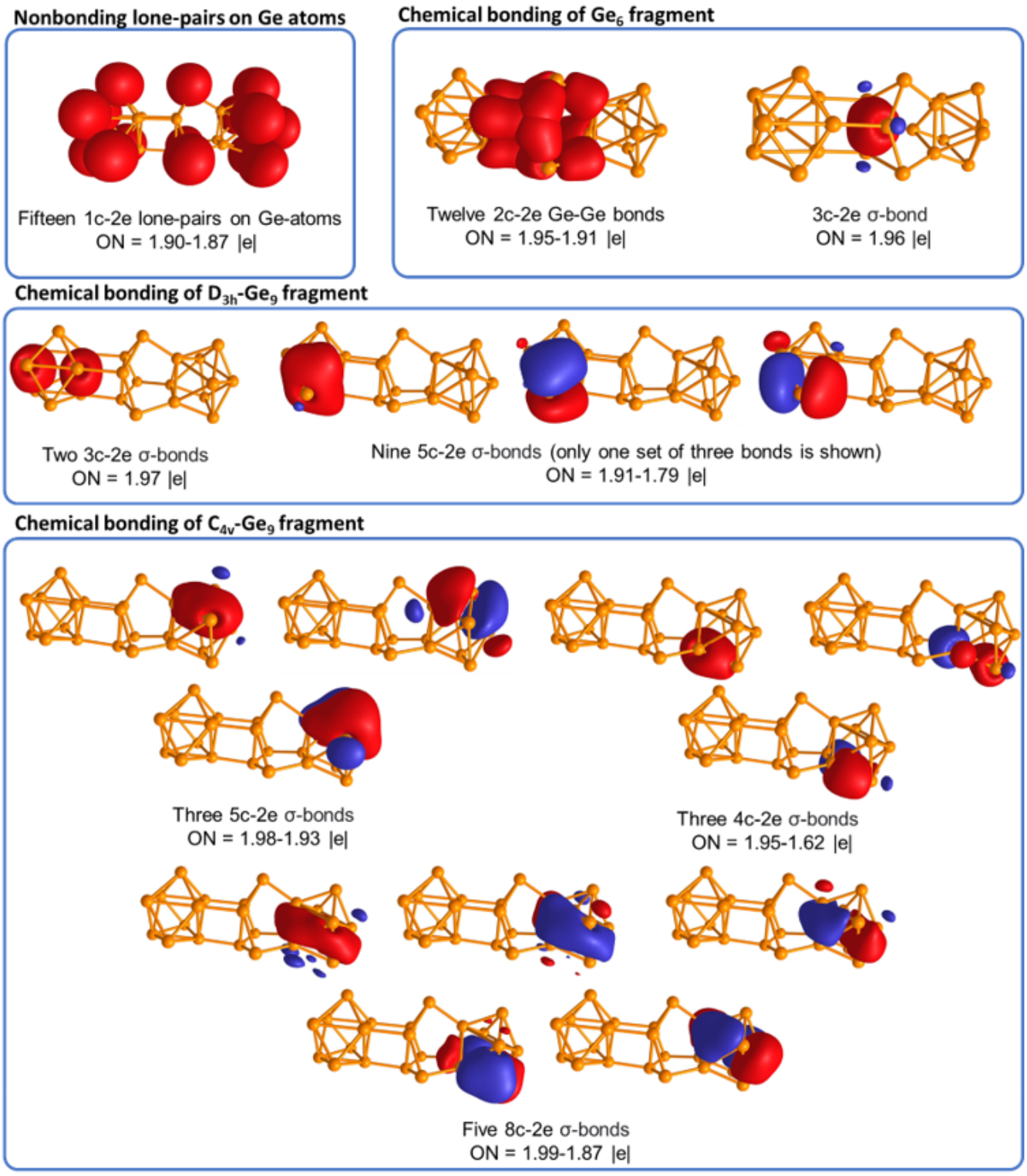

Figure 2

Chemical bonding pattern of Ge244- cluster. Different phases of a wave function represented with different colors. Positive: red; negative: blue.

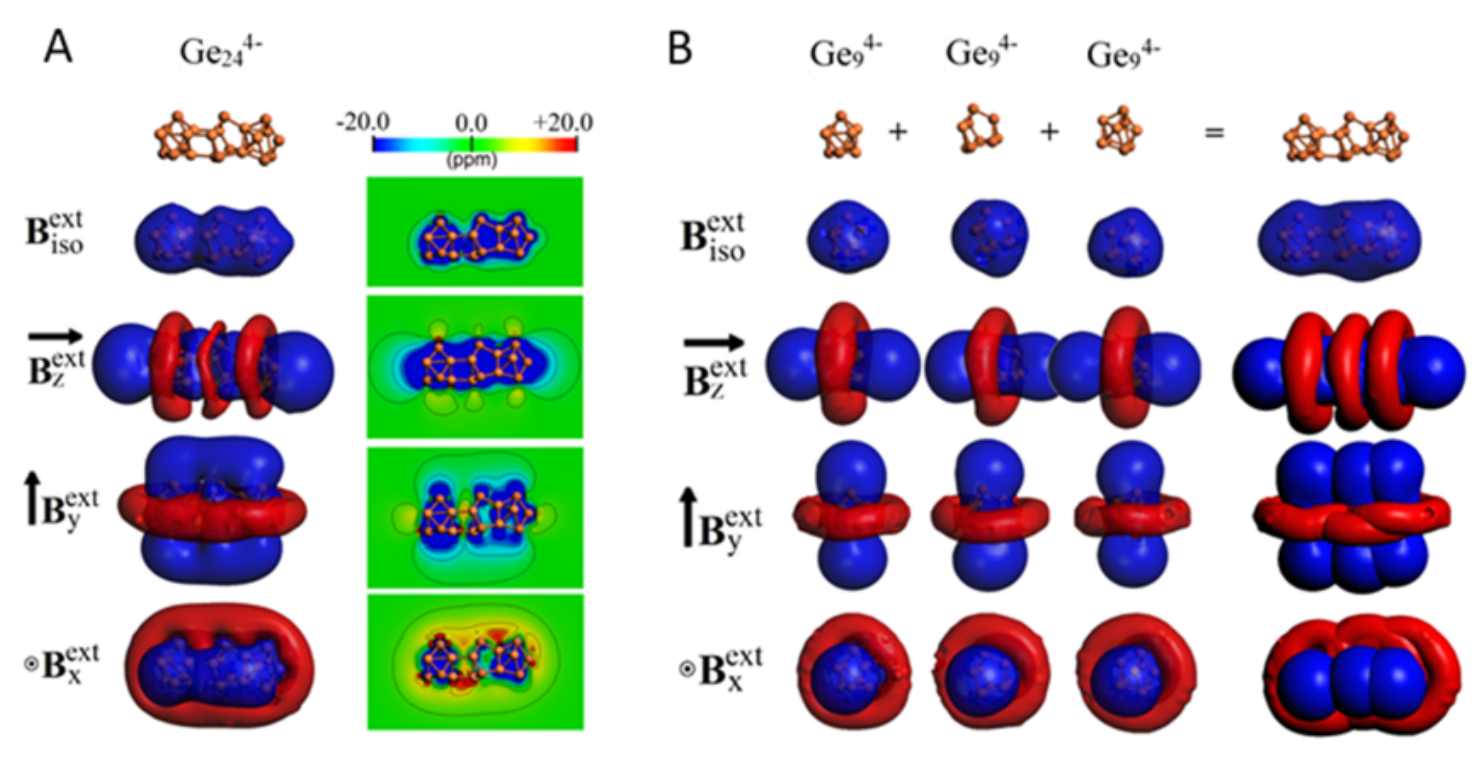

Figure 3

(A) Isosurface and contour plot representation for Bisoind and certain orientations of the external field for Ge244-. Isosurface value set at ±3.0 ppm. (B) Isosurface representation for Bisoind and certain orientations of the external field for the three isolated Ge94- units, as found in Ge244-. Isosurface value set at ±3.0 ppm.

Supplementary Files

This is a list of supplementary files associated with this preprint. Click to download.

- Ge244checkcif.pdf
- SupplementaryInformation.docx
- GraphicalAbstract.png